The potential of flax shives as reinforcements for injection moulded polypropylene composites

Lucile Nuez, Johnny J. Beaugrand, Darshil Shah, Claire Mayer-Laigle, Alain Bourmaud, Pierre D'arras, Christophe Baley

The potential of flax shives as reinforcements for injection moulded polypropylene composites

Lucile Nuez[1,2*], Johnny Beaugrand[3], Darshil Shah[4], Claire Mayer-Laigle[5], Alain Bourmaud[1], Pierre D'Arras[2] and Christophe Baley[1]

1 : Université de Bretagne-Sud, IRDL, CNRS UMR 6027, BP 92116, 56321 Lorient Cedex, France

2: Van Robaeys Frères, 83 Rue Saint-Michel, 59122 Killem, France

3: Biopolymères Intéractions Assemblages (BIA), INRAE, Rue de la Géraudière, F-44316 Nantes, France

4: Centre for Natural Material Innovation, Department of Architecture, University of Cambridge, Cambridge CB2 1PX, United Kingdom

5: UMR 1208 IATE, Cirad, INRA, Montpellier SupAgro, Université de Montpellier, 2 place Pierre Viala, 4060 Montpellier Cedex 02, France

* Corresponding author:*e-mail address* alain.bourmaud@univ-ubs.fr

Tel.: +33-2-97-87-45-18; Fax: +33-2-97-87-45-88

Abstract

Flax shives (FS) represent approximately 50% in weight of dry flax stems, making it the main by-product of the flax scutching industry. Being an available and low-added value lignocellulosic resource, flax shives are an interesting candidate for thermoplastic composite reinforcement. In this study, raw flax shives were fragmented by knife milling using two grids of 500 and 250 µm respectively, while a third batch, with a targeted particle size below 50 µm, was obtained by an attrition beads mill. The fragmentation methods used do not modify the biochemical composition of FS but do reduce their crystallinity due to both crystalline cellulose allomorph conversion and amorphization. The poly-(propylene) and 4%-wt maleic anhydride modified poly-(propylene) injection moulded composites produced with these reinforcing materials have a maximum tensile strength that evolves linearly with particle aspect ratio after processing. The tensile Young's modulus of the composites reinforced by coarser particles is 3268 ± 240 MPa, which is almost 90% that obtained for a reference 1 mm flax fibre reinforced composite. Furthermore, a basic micromechanical model was applied highlighting the reinforcing capacity of cell wall-like small tubular structures (e.g. flax shives). This study underlines the reinforcing potential of low-value by-product flax shives for value-added composite applications.

Keywords

Flax shives, injection moulding, morphology, mechanical properties, X-ray diffraction

1. Introduction

The development of the biocomposite industry in the past few decades due to ecological concerns has notably contributed to a growing interest in the plastic composite reinforcing potential of various agricultural by-products such as woody hemp core [1], sugarcane bagasse, sunflower and corn stalk [2], rice hull, corn cob and walnut shell flour [3]. Driven by eco-responsibility reasons such as the reduction of synthetic petrochemical consumption, the use of agricultural by-products represents a potential economically viable solution for local economy waste management, so long as transportation and transformation costs are limited. As flax cultivation areas are increasing (+8% in France from 2017 to 2018), so are the quantities of agricultural by-products from the flax scutching industry. Flax shives might then even be an alternative to the widely used wood flour in wood plastic composites (WPC), and their addition to wood flour could contribute to reducing the cost of such materials alongside recycling waste. Indeed, flax is an annual plant which temporarily stores carbon dioxide during growth [4, 5]. In the case of France, the flax cultivation areas are geographically concentrated along the English canal (from Normandie to the North), and this is a major advantage for material transportation from the production site to the end-use factory.

When cultivated for its fibre, flax stems are grown to be approximately one metre in height with a diameter of up to 3 mm [6]. When mature, stems are harvested, undergo a retting step followed by a scutching process in order to extract the high added-value bast fibres. The retted stems are crushed by successive fluted rollers, and then beaten from bottom up in order to separate the fibres from the rest of the stem constituents, mainly from flax shives (FS) which are a cause of quality defects in the fibre transformation processes. FS represent around 50% in weight of retted flax stems [7], which makes them the main by-product of the flax fibre production process. Traditionally used for soil amendment, animal bedding or particle boards for building insulation [8], FS have also been studied as a resource for various innovative applications including activated carbon [9], 3D printed lightweight concrete [10], and bio-fuel production [11]. FS have a low added value, a low density and, above all,

60 are a widely available resource which flax scutching companies wish to broaden the areas of
61 application of, and this makes them a genuine potential reinforcing material in bio-composites.
62 Flax shives, also referred to as woody core, have a highly lignified structure made of the inner tissues
63 of the stem, namely the pith, the xylem and the phloem, the last two having a role in the conduction of
64 raw and elaborated sap, respectively. Studying the transverse section of flax stems, Goudenhooft et
65 al. measured the tissue content to be between 70 and 85% depending on the flax variety, and the
66 xylem represents about 75% of the total tissue content [6, 12]. They also found, by stem flexural
67 bending tests, that the woody core has a structural role and accounts for up to 30% of dry flax stem
68 bending stiffness due to architectural differences and lower density.
69 The composition of flax shives is approximately 25% lignin, 50% cellulose, and 20% hemicellulose [3,
70 13], but this varies depending on the analytical method, plant maturity and even location of FS in the
71 stem. Day et al. [14] found that lignin content ranges from 24% to 32% in the inner tissues depending
72 on maturity and location in the stem, against only 1.5% to 4.2% in the dry cell wall resides in the outer
73 tissues (specifically fibre bundles imbedded in the parenchyma, the cortical parenchyma, and the
74 phloem).
75 Raw bulk flax shives demonstrate a considerable particle size distribution, with particles as long as
76 40 mm [10] and thus can be difficult to use as such for efficient polymer reinforcements. Consequently,
77 a mechanical size reduction step such as comminution by grinding is useful in controlling particle
78 granulometry, size distribution and aspect ratio (ratio of length over particle width or fibre diameter).
79 Knife milling can be used as a first reduction step (from the meter scale to that of the centimetre) of
80 forages or stems [15]. In this grinder, particles are fed continuously and the comminution is mainly
81 achieved by shear mechanisms. The size of the ground particles is determined by the size of the hole
82 of the sieving grid (from a few millimetres to hundreds of micrometres) at the output of the milling
83 chamber. On the other hand, small particles (10-500 µm) can be obtained by media milling, which
84 consists of breaking down batches of particles by compression and attrition mechanisms thanks to a
85 milling media (ball or beads) put in motion by a rotor, a vibrating or rotary tank. This technique allows
86 to reach very fine particles but the total energy consumption is higher due to long residence time
87 required to obtain such fine granulometries [16]. In addition it has also been proven that such
88 technologies reduce the crystallinity of plant cell wall cellulose [17, 18].

In composites, the bonding efficiency will determine the quality of stress transfer between reinforcement and matrix. When plant fibres are embedded in a polymer matrix, they generally increase its stiffness and reduce tensile deformation. An optimal fibre volume fraction has been observed in injection moulded PP composites after which tensile strength decreases; this is around 33%-vol specifically in the case of flax-PP composites [19, 20, 21]. The impact of reinforcing fibres on composite mechanical properties depends in particular on fibre orientation which in the case of short fibre reinforced injection moulded composites depends on the severity of the skin-core effect. Morphology and structure of plant reinforcement also plays a major role in fibre orientation [22]. Fibre length, tendency of packing, viscosity, process parameters, all influence the thickness of the skin layer which contains the most fibres parallel to the melt flow direction and accounts for higher mechanical properties [22, 23, 24]. The higher the fibre aspect ratio, the higher the mechanical properties. Stark et al. [25] compared the role of wood flour and wood fibre having approximate aspect ratios of 4 and 16 respectively. When incorporated with MAPP in injection moulded composites, they found that tensile strength of the latter increased between 30 and 60% depending on the amount of wood fibre compared to wood flour composites. While the aspect ratio of flax fibres will depend on fibre fineness and processing [26, 27], that of flax shives will depend highly on the mode of comminution.

The aim of this study is to evaluate the reinforcing potential of flax shives, a by-product of flax fibre crop. In order to situate the mechanical properties of FS injection moulded PP composites, a panel of different plant cell walls were tested for comparative purposes. This analytical investigation is based on a two-level strategy. First, the FS structure was examined by particle size analysis following two methods of comminution (knife or attrition beads milling). An ultrastructural study of these fragmented FS was carried out by X-ray diffraction analysis. Additionally, the constitutive polymers of FS were characterised by biochemical analysis. Second, at the scale of the composites, mechanical properties of injection moulded composites were measured, specifically interrogating the impact of FS particle size and filler volume fraction (from 0% to 31%). Finally, a theoretical approach to determine FS critical length was discussed with the help of a simplified mechanical model, to understand the reinforcing potential of small and hollow cell wall structures such as shives.

2. Experimental

2.1. Matrix polymer

The matrix used in this study is polypropylene, chosen because it is a commodity polymer widely used in the automotive industry. PPC 10642 was supplied by Total Petrochemicals (France) with a MFI of 44 g/ 10 min at 230°C and 2.16 kg, and a polymer density of 0.94. Because plant cell walls have an important polysaccharide content giving them a hydrophilic nature, maleic anhydride modified polypropylene (MAPP) was added to the formulation as compatibilizer for its amphiphilic nature enabling bonding with both the hydroxyl groups of the filler and the hydrophobic polymer matrix [28]. MAPP (Orevac CA 100) was supplied by Arkema (France) and has an MFI of 10 g/10 min (at 190 °C and 0.325 kg), 4% of MAPP were added to the formulation during the compounding process as it represents a good compromise between bonding improvement and cost of polymer [29].

2.2. Reinforcing materials

The flax shives used in this study were provided in bulk by the flax scutching company Van Robaeys Frères (France) following the scutching of the 2018 flax harvest year, before being milled with a laboratory scale rotating cutting mill (Retsch Mühle, Germany). The mesh size of the grids used were either 500 µm or 250 µm. To obtained finer powder, the powder ground with the knife mill (250 µm-grids) have been submitted to an additional milling step in an attrition beads mill, as the previous technique is not adapted to obtain such fine granulometries [30]. The equipment employed is a laboratory prototype, composed of a milling chamber of 3 L in which 175 g of the powder to grind and 7.5 kg of small steel beads (6 mm) are put in motion by a rotor at 300 rpm. The milling time (100 min) was determined so that at least 90% of micronized particles have a diameter below 50 µm.

The flax fibre (*Linum usitatissimum L.*) used is from the Alizée variety, which was harvested in 2017 in Normandy (France), and was scutched and hackled before being cut to 1 mm in length and supplied as such by Depestele (France). In the rest of this study, the term “fibre” will designate both elementary fibres and flax fibre bundles as both are present in the studied batch; otherwise differentiation will be made by specifying “elementary fibres” or “bundles”.

An additional sample of wood flour was studied for comparative purposes as it is commonly used in the wood plastic composites industry. This sample is composed of a mixture of untreated *pinus pinaster* and *picea sitchensis* wood chips originating from sawmill residues, therefore precise history

147 and composition is unknown. They have further been dried, fragmented by hammer milling with a 1
148 mm grid and sieved. The fraction under the 800 µm sieving mesh size was studied here. All reinforcing
149 materials and their corresponding abbreviations as they will be used throughout the article are given
150 Table 1.
151
152 *2.3. Particle size analysis*
153 Particle morphology was studied by a dynamic image analysis device, QICPIC (SympaTec GmbH,
154 Germany). Two shape factors were determined (i) the particle length, defined as the shortest path
155 between the most distant end points of the particles after skeletonization, (ii) an aspect ratio (length
156 over diameter). The aim was to understand the effects of comminution on the granulometry of FS.
157 Both the materials samples before and after extrusion and injection moulding (see section 2.6) were
158 investigated. For the latter, samples were obtained from composites after dissolving the PP matrix with
159 o-xylene at 150°C during 3 days by reflux. The extracted particles were then thoroughly washed with
160 boiling xylene followed by acetone and left to dry overnight in a 60°C oven. All samples were oven
161 dried at 60°C overnight before measurement in order to limit analysis bias caused by initial water
162 content. Two protocols have been adapted for the particle morphometric description by the QICPIC.
163 For the raw particles (flax shives and flax fibres), the most appropriate way was to disperse those
164 samples with a vibrating chute VIBRI unit combined with a dry dispersion unit GRADIS, because of
165 their important particle size and easy scattering. All the others samples micronized or extracted from
166 composites were more appropriately analysed with a liquid dispersion unit, MIXCEL. Indeed, these
167 batches displayed a tendency to particle aggregation so they were first dispersed in ethanol. To obtain
168 accurate data in the morphological measurements, the QICPIC lenses (from M9 to M5) have been
169 adapted to the size of each sample. The selection of the appropriate lens is based on initial visual
170 coarseness of sample and supplier specifications. As we assume that the particle size variation
171 remains weak before and after processing, the same lens was used in this case in order to obtain data
172 in the same range. The number of analysed particles varied between 20,000 and 10 million depending
173 on samples, measurements were made in triplicates to ensure reproducibility of the results. PAQXOS
174 software (SympaTec GmbH, Germany) was used to calculate particle length and aspect ratio in real
175 time.
176

2.4. Biochemical composition

The monosaccharide content of the sample lots (Table1) were assessed by wet chemical analysis, aside from the extracted ones after extrusion-injection because of arguable extraction bias due to the o-xylem solvent used. Before hydrolysis, the large size of the R-FS, FF and WF particles requires a first step of homogenization done by cryogrinding (SPEX 6700 freezer Mill) of approximately 1g of materials. The whole panel of powdered samples (approx. 5 mg per assay) were then hydrolysed in 12 M H2SO4 (Sigma Aldrich) for 2 h at 25°C (heat plate) followed by additional hydrolysis of 2 h at 100°C with 1.5 M H2SO4 in presence of inositol as internal standard. Galacturonic Acid (GalA) and Glucuronic Acid (GlcA) was determined by an automated m-hydroxybiphenyl method [31] and merged as Uronic acid (UrAc), whereas individual neutral monosaccharides (arabinose, rhamnose, fucose, glucose, xylose, galactose and mannose) were analysed as their alditol acetate derivatives [32] by gas-liquid chromatography (Perkin Elmer, Clarus 580, Shelton, CT, USA) equipped with an DB 225 capillary column (J&W Scientific, Folsorn, CA, USA) at 205°C, with H2 as the carrier gas. Standards of carbohydrate solutions with three known concentrations were used for calibration. Analyses were performed in three independent assays. The total monosaccharide content is the sum of each monosaccharide amount, and is expressed as the percentage of the dry matter mass.

The lignin content was quantified in the panel of samples (Table 1) from the homogenised micronized particles. Lignin was quantified by colorimetrical analysis following the acetyl bromide method [33] on mass weight samples of approx. 20 mg per essay. The chemicals were laboratory grade from Sigma Aldrich and the analyses were performed in at least three independent assays, with lignin expressed as the percentage of the dry matter mass.

2.5. X-Ray Diffraction

Wide-angle X-ray diffraction (XRD) measurements were performed in triplicates under ambient conditions on a Siemens D500 diffractometer CuKα radiation. Samples were loaded on a silicon wafer and scans were collected from 2θ = 10 to 30° with step size of 0.03° at 2 s/step, at 30 kV and 20 mA. Crystallinity was calculated based on the method developed by Segal et. al using Eq. 1, where I_{tot} is the intensity at the primary peak for cellulose I (at 2θ ≈ 22.5°) and I_{am} is the intensity from the amorphous portion evaluated as the minimum intensity (at 2θ ≈ 18.5) [34][35].

$$C = \frac{I_{tot} - I_{am}}{I_{tot}} \times 100 \quad \text{(Eq. 1)}$$

2.6. Preparation of composites

Before processing, the reinforcing materials and PP-MAPP matrix were oven dried at 60 °C for at least 12 hours. They were then compounded with a single-screw extruder (Fairex, England) at 190 °C and an extrusion speed of 25 rpm. The length and diameter of the screw were 600 and 20 mm respectively, inducing an aspect ratio L/D of 30. After granulation and oven-drying in the same conditions, the material under-went a second extrusion step using a TSA (Italy) co-rotating twin-screw extruder with a screw diameter of 20 mm and L/D ratio of 40. A temperature profile going from 180°C to 190°C and a die temperature of 180° C were imposed with a screw rotation speed of 300 rpm. The material was once more granulated, oven-dried, and ISO 527-2 type 1B normalised specimens were obtained using an 80 Tons Battenfeld (Austria) injection moulding machine with a constant barrel and mould temperature set at 190°C and 30 °C, respectively.

2.7. Mechanical Characterization

The injection moulded T-bone specimens were submitted to tensile testing following the ISO 527 standard on an MTS Synergie 1000RT machine with a controlled environment (temperature of 23°C and relative humidity of 48%). Tensile speed was of 1 mm/min and nominal gauge length was 25 mm. A 10 kN sensor was used to measure the applied force on the specimen, and an extensometer was used to measure deformation during the tests.

2.8. Density measurements

The density of raw FS-500 was measured by helium pycnometer measurements based on the method described by Le Gall et al. [36]. Measurements were made in 10 replicates and the average value of 1.43 g/cm^3 was obtained. The rule-of-mixtures was then applied to calculate the volume fraction in the composites knowing the density of the PP-MAPP matrix as follows (Eq. 2):

$$\rho_c = \rho_{fs} V_{fs} + \rho_m (1 - V_{fs}) \quad \text{Eq. 2}$$

With ρ_c, ρ_{fs}, and ρ_m the density in g/cm^3 of the composite, the flax shives and the matrix respectively, and V_{fs} the volume fraction of the reinforcing flax shives, calculated knowing the mass fraction and density of the components.

2.9. SEM Observations

The raw reinforcing materials were observed using a Joel JSM 6460LV (France) scanning electron microscope (SEM) after comminution and prior to composite processing after being sputter coated with a thin layer of gold in an Edwards Sputter Coater. The fracture surface of specimen following tensile testing were also observed by SEM.

3. Results and discussions

3.1 Characterization of the reinforcing materials

3.1.1 Validation of the experimental procedure

First, a comparison between the number and volume length distributions is proposed in order to determine a valuable method of particle size analysis using the dynamic analyser used (QICPIC). Particle morphology analysis provides significantly different information depending on measurement parameters such as equipment used, image resolution, automatic or "by-hand" measurements, causing specific particle size populations to be potentially left out [36, 37, 38].

The length distributions given in number and volume are schematically displayed by box-plot diagrams in Figure 1. Because a unique average value does not give any information on distribution span, symmetry, skewness or extreme values, box plots are preferred. It is a simple visual tool adequate to use in statistical analysis to evaluate data (median, span…) without making any suppositions on its distribution, especially when it does not follow a normal or log-normal law. The 10th (first decile), 16th, 50th (median), 84th, and 90th (last decile) percentiles of the cumulative distribution in length are shown respectively from bottom up.

The number distributions (Fig. 1a) emphasise the quantity of small particles present in each batch, as each particle is given the same "weight" regardless of size. On the contrary, in the volume distribution (Fig. 1b), a "weight" is attributed to each particle corresponding to the volume of the particle divided by the total volume of particles analysed. In this study, the particle volume is assimilated to a cylinder of

263 which the length and diameter are those measured for each particle. Therefore, in this distribution
264 small particles are somewhat obscured as their weight is much lower than that of larger particles.
265 Both the distribution in number and in volume are complementary for readers to have a cognitive
266 understanding of a population of particles, however in the aim of materials reinforcement when dealing
267 with natural fibre, the distribution in volume is most desirable compared to the distribution in number
268 [40] as this parameter is most representative of the volume fraction of reinforcing material and its role
269 in the mechanical support of the composite.
270 Note also that small particles are composed of only few pixels and the precision in the determination of
271 the shape factors are lower than for larger particles like fibres composed of hundreds of pixels. By
272 choosing an adequate lens for the device, it is possible to increase the number of pixels of an element
273 thanks to a shorter length scale of the pixel size, but in this case, it becomes difficult to focus on larger
274 particles. Thus, for powders exhibiting broadly scattered particle sizes, the limitations of the device do
275 not allow to have a high resolution for both small and large particles at the same time. This point
276 should be kept in mind when comparing the different particle size distributions.
277 Figure 1a reveals that 84% of raw flax shives (R-FS) are made up of particles less than 90 µm long,
278 whereas the volume distribution shows that 16% of particles are less than 3052 µm long. Except for
279 FS-50, all initial reinforcing materials have at least 80% of their number distribution which lays
280 completely out of their volume distribution. Shives are obtained during the scutching of flax, which also
281 produces up to 10%-wt of dust from the retted straws originating mainly from cultivation step in the
282 fields. An unknown part is left in the shives and is found in the initial R-FS and will be present in all
283 batches as it won't be affected by comminution. This proportion of particles smaller than 200 µm
284 (which represents the particle length limit commonly admitted as defining fines [41]) is present in all
285 studied reinforcing materials as the FS-500, FS-250 and FF median lengths in number are of 8 or 9
286 µm against 484 µm, 455 µm, and 976 µm in volume respectively.
287 The sample length distributions in volume (Fig. 1b) shows the initial R-FS median length is reduced by
288 10 when using the knife-milling step in the case of FS-500. The latter's median length is then
289 comparable to that of the FS-250 sample at 455 µm. The 84^{th} percentiles of FS-500 and FS-250 are at
290 1518 µm and 1134 µm respectively, which is respectively 3 and 4.5 times more important than the
291 initial milling grid mesh size. This can be explained by the grids' pattern which has a grating effect on

292 R-FS. Furthermore, the 84th percentile of FS-50 is of 30 µm, making the length of this sample
293 complementary to that of the last two samples for this study.
294 The morphological study of particles can be carried out by image analysis after observation under
295 optical microscope of a sufficiently significant population of particles. Automated laser measurements
296 have the advantage to be less operator dependant. Le Moigne et al. [37] found that 'by hand'
297 measurements induced a discrepancy and had a tendency to magnify fibre dimensions due to
298 operator dependence compared to using a specific software for fibre detection (50% of the number
299 weighted length of flax fibres measured by hand were more than twice the length of the same particles
300 detected by the software). Dynamic image analysis is a time-efficient method to obtain a wide amount
301 of particle morphology information such as shape descriptors and distributions in number, length,
302 surface or volume [38]. In the rest of this study, analysis is carried out on the basis of volume
303 distributions.
304
305 ### 3.1.2 Morphological analysis of raw reinforcing materials
306 Figure 2 shows the particle length distribution in volume as well as the overall aspect of the reinforcing
307 materials as observed with SEM images. Prior to comminution, R-FS presents a very wide fibre length
308 distribution with a median of about 4850 µm and a main mode at 6300 µm, which is similar to the "by-
309 hand" optical measurements by Evon et al. [42] of 5800 ± 4013 µm of average length. The reference
310 flax fibres present a homogeneous fibre length with a unimodal distribution having a median of 976 µm
311 coherent with the targeted fibre length of 1 mm. Wood flour exhibits a heterogeneous length
312 distribution, with a visually important aspect ratio, and a median length of 440 µm. Wood flour used in
313 this study originates from saw milling waste and was used as-received without any further sieving.
314 FS-500 and FS-250, both fragmented using a knife milling device and milling grids of 500 µm and 250
315 µm respectively, show several distinct particle populations: fine particles having a mode at
316 approximately 70 µm for both samples, and coarser particles with a mode of 1450 µm and 1000 µm,
317 respectively. This similar behaviour can be explained by the comminution process for which raw FS
318 are continually fed to the machine inducing an unknown residence time, causing certain particles to be
319 more fragmented than others. In addition to this, we can assume that depending on the origin of FS
320 (e.g. type of cell, position in the plant, plant maturity), the differences in cell wall rigidity (varying
321 amount of lignification depending on the role of the cells in the plant) and specific mechanical strength

of initial R-FS will have an effect on the kinetics of fragmentation and disaggregation. Flax xylem compressive strength at break measured from 3-point bending tests carried out on peeled flax stems is approximately 60 MPa, which is a third of the strength of the whole stem [43]. The mostly xylem origin of FS also explains why the fine particle population visible on the SEM images of both FS-500 and FS-250 is absent in that of FF. Furthermore, contrasting initial processing steps may bring further insight on this phenomenon as flax fibres were hackled before being cut, which further removes residual cortical tissues from fibre bundles and therefore reduce the amount of fines in the sample. Figure 3 shows that the alveolar structure of FS from the plant's xylem is preserved after knife-milling providing a reinforcing material with hollow tubular sections corresponding to dry conduction vessels or supporting xylem cells. Indeed, in a knife mill, the compression mechanism remains weaker in comparison to shear mechanism and the type of mill is known to preserve the structure of the plant materials [44].

Furthermore, Figure 2 shows that particle length distribution of FS-50 is very narrow, with a first decile, a median, and a last decile of 9 µm, 17 µm, and 33 µm respectively, accounting for a homogeneous particle fragmentation justified by the intensity of the 23-hour ball milling process. This panel of results exhibits the strong impact of the material preparation (cutting, knife milling, or ball milling) on particle morphology and structure.

3.1.3 Biochemical analysis

The monosaccharide and lignin content of the different samples are given Figure 4. Considering that glucose accounts for sample's content in cellulose, then flax fibres FF are made of 70% of cellulose on average (out of total dry matter content) compared to only 30% for flax shives FS and 42% for wood flour WF; and approximately 3% of lignin for FF, against 30% for WF and R-FS. The latter also contain about 16 times more xylan than FF which is in agreement with measurements carried out by Buranov et al. [30, 44]. The differences in biochemical composition can be explained by the contrasting origins and functions of cells in the flax stem. Due to their high mechanical role, flax fibres possess well developed secondary cell walls made up of cellulose microfibrils and can be considered as gelatinous fibres [46] with low lignification. In contrast, xylem cells have a role in the mechanical support of the plant and so have a secondary cell wall, but are responsible for raw sap conduction and therefore are

highly lignified from the base to the top of the plant [47], also highlighted by the progressive lignification of the xylem throughout plant growth [14].

Since the wood flour comes from fluctuant sawmill wastes, it is a blend of both soft and hardwood but the precise species origin is unknown, as well as its ratio. Therefore its biochemical composition was determined for information purposes and is in agreement with ranges found in the general literature [48].

Furthermore, the amount of cellulose, lignin and non-glucosidic monosaccharides does not significantly evolve in the FS samples following fragmentation, even in the case of intense milling in the attrition beds mill (FS-50). It is interesting to notice that contrary to ball milling known to cause a drop in cellulose content in wood or flax fibres, the intense milling employed here seems to preserve the total chemical composition of the powder. This is probably due to the shorter milling time (100 min compared to several hours in ball milling).

3.1.4 XRD

The diffraction pattern of cellulose I (Fig. 1a) includes five major reflections for the crystalline phases at $2\theta \approx 15°$ ($1\bar{1}0$ diffraction plane following the recommendations of French [49]), 17° (110), 21° (102), 22.5° (200) and 34.5° (004), with the amorphous phase observed at $2\theta \approx 18.5°$ [35]. These reference peaks were used to analyse the XRD spectra of the various flax fibre samples (Fig. 5a).

All samples exhibit a primary peak at $2\theta \approx 22.5°$ corresponding to the crystalline 200 plane of cellulose I, however the peak is sharp and distinct for raw flax fibres, slightly broader for raw flax shives until $2\theta \approx 12°$ (belonging to cellulose II or III), supposing the presence of both cellulose I and cellulose II or III in raw flax shives. This peak gets broader (left-ward) with the severity of attrition beads milling (Fig. 5a). In addition, raw flax fibres, and to an extent raw flax shives, exhibit the $1\bar{1}0$ and 110 secondary peaks, while these peaks are less distinct for ball milled flax shives, and not discernible for FS-50. The noted qualitative observations and subsequent measurements (Fig. 5b) suggest a reduction in crystallinity (increase in level of disorder) of the shives with severity of ball milling, as was observed with after two hours of ball milling on crystalline cellulose [50]. Specifically, while raw flax fibres and shives have a crystallinity of 77.2% and 60.0%, respectively, the cellulose crystallinity reduces to 41.7%, 38.8% and 28.9% for FS-500, FS-250 and FS-50, respectively. The latter is comparable to the crystallinity of wood flour (31.3%).

With increasing severity of ball milling, while no distinct shifts in diffraction peaks are observed, there is left-ward broadening of the 2θ ≈ 22.5° (belonging to 200 plane of crystalline cellulose I), and the presence of an additional and increasingly important peak at around 2θ ≈ 12° (which belongs to cellulose II or III) [51]. Notably, wood flour exhibits this prominent peak as well (Fig 5a). These indicate that cellulose II or III is becoming prominent with ball milling; typically, cellulose I irreversibly converts to cellulose II upon mercerisation or urea treatment [50, 51], and cellulose I can reversibly convert to cellulose III upon liquid ammonia treatment [52, 51]. Notably, there are a number of studies which have reported the conversion of cellulose I into cellulose II,III or IV after ball milling under specific conditions [17, 53, 51]. In particular wet ball-milling using water [17, 54, 55, 56] (or NaOH/urea) [53], even at ambient temperatures (25 °C), can partially transform cellulose I to cellulose II relatively quickly (e.g. 30 minutes of ball milling). Higher temperatures (e.g. 80 °C and above) can further assist the transformation, particularly into cellulose IV [17]. The temperature of the powder measured at the end of the milling step in attrition beads mill was of 70 °C and could explained the change observed in the crystallinity of the cellulose. In our studies, we haven't measured how temperature evolves during knife milling.

Comminution, by amorphization of particles, results in a decrease in degree of polymerization and therefore of sample crystallinity. But the comminution process parameters (temperature, humidity, milling media) also impact cellulose type conversion that are revealed here. These crystallinity modifications have an effect not only on material sensitivity to moisture absorption but also on sample thermal stability and adhesion with the polymer matrix and thus composite mechanical properties.

3.2 Properties of composites

3.2.1 Reinforcement material morphology analysis after processing

Before evaluating the mechanical properties of the PP-MAPP injection moulded composites processed with 30%-wt reinforcing materials, the morphology of the reinforcing particles after processing are given in Figure 6a and b. Figure 6a shows that FF, the 50/50 mix of FF and FS-500 and FS-500 have important length spans with a median length of 289 µm, 317 µm and 297 µm respectively. The 90th percentile of these samples increases in the same order, indicating an important number of long particles present in the FS-500 sample which explains that FS-500 + FF has a higher median than FF itself.

411 The length of FF presents a drastic drop of 70% after processing from their initial length given in figure
412 1b. The twin-screw extrusion is assumed to be the cause of this as it generates high shear stresses
413 [20]. Some authors have studied this effect and reported a length reduction between 50% and 70% of
414 average flax fibre initial length after mono-screw extrusion processing [22, 40]. As shown in Figure 7,
415 the twin-screws used in this study are designed with several kneading areas, one of them being even
416 reversed, leading to improved mixing and additional shear stresses. Furthermore, defects in flax fibres,
417 known as “kink-bands”, have been shown to influence the rupture of fibres during compounding as
418 localized stress concentrations cause fibre rupture after processing to coincide with the mean distance
419 between two consecutive kink-bands [57, 58].
420 Surprisingly, FS-500 only underwent a 39% median length reduction due to processing, and an
421 important quantity of longer particles is present after processing when compared to FF. Shives consist
422 of fragmented assemblies of xylem cells, which are highly lignified in contrast to fibres. Even so, FS-
423 250 and WF underwent a 75% and 70% decrease in length respectively, therefore the fragmentation
424 mechanisms of the FS-500 sample are complicated to judge without further analysis. Moreover, the
425 proportion of smaller particles is less affected by shear stresses: this is clearly visible in the case of
426 FS-50 as their length distribution stays practically unchanged with a median length of 20 µm before
427 and after processing. This suggests that the process may reduce particle length up to a critical length
428 independent of initial fibre length number of processing cycles.
429 Figure 6b shows the evolution of the distribution of particle aspect ratio before and after processing. It
430 is possible to see a 36%, 40 % and 77% decrease between Raw-FS and FS-500, FS-250 and FS-50
431 respectively depending on comminution mode. The median aspect ratio of WF is of 5.5, which is
432 comparable to that of FS-250, but to the limit that WF shows a higher amount of high aspect ratio
433 particles, as the WF last decile is of 15.4 against 11.9 for FS-250. After processing of the 30%-wt
434 reinforced PP-MAPP composites, reinforcement material aspect ratio globally decreases. Indeed, the
435 L/D of FF and WF decreases by 8% and 11% when compared to before processing, and this is even
436 more accentuated for FS-500 and FS-250, which show a 21% and 38% drop respectively.
437 Interestingly, L/D distribution tends to tighten for FS towards smaller values due to the reduction of
438 particle length because during processing, as discussed earlier.
439 The median aspect ratio of FF is the highest at 11.5 due to the combined action of the delamination
440 of bundles into individual fibres [37]. For the other reinforcing materials, the median aspect ratios are

441 of 4.8, 3.5 and 2.3 for FS-500, FS-250 and FS-50 respectively, while that of WF is equivalent to FS-
442 500 at 4.9, although a higher proportion of elongated particle is present as the 84th percentile is of 8.4
443 for WF against 7.3 for FS-500. Flax fibres therefore have a load transfer potential more than twice as
444 great as wood flour but other parameter must be taken into account such as fibre-matrix adhesion and
445 the proportion of fines possibly accountable for fracture initiation. The relevance of the 50/50 mixture
446 of FF and FS-500 is to increase by 30% the median aspect ratio of FS-500 and by up to 110% the last
447 decile, meaning the potential load transfer of the material is highly improved all the while the price of
448 the raw material is considerably diminished compared to the initial cut fibres. Indeed, the market value
449 of raw flax shives can be as low as one thirtieth that of scutched flax fibres. Furthermore, varying
450 proportions of FS and FF would allow for specific composite mechanical properties all the while
451 controlling the reinforcing material's cost.
452
453 ### 3.2.2 Tensile properties
454 Table 2 shows the tensile mechanical properties of the injected composites of PP-MAPP matrix
455 reinforced with 30%-wt of the different reinforcing samples. As expected, the incorporation of flax
456 shives results in a general increase of tensile Young's modulus and maximum strength. The Young's
457 modulus increases from + 46% to + 112% when FS-50 and FS-500 respectively are compared to the
458 reference PP-MAPP matrix. FS-500 have a modulus of 3268 (± 240) MPa, which is 90 % that of the
459 FF reinforced composite, and more than a 110% increase in composite rigidity when compared to the
460 WF reinforced PP-MAPP. Moreover, the addition of flax fibres in the FS-500 reinforcing batch does not
461 considerably modify the composite's rigidity.
462 Furthermore, the composites have an overall dissimilar ultimate strain. FS-250 and FS-500 have a
463 comparable behaviour with small ultimate strains of approximately 2.3% as shown Figure 8a and
464 Table 2. FS-50 and FF+FS-500 both have an ultimate strain 52% higher, while WF and FF exhibit an
465 increase of 109% and 139% respectively given the ultimate strain of the pure matrix of about 11%.
466 Finally, FS-50 enables a 27% increase in maximum tensile strength when compared to the initial PP-
467 MAPP matrix, while FS-250 and FS-500 have a similar behaviour with values around 25 MPa. When a
468 50/50 mix of FF and FS-500 is incorporated, a 10% increase in tensile strength is noted, reaching and
469 slightly exceeding that of WF. FS-500 enables the composite to reach almost 80% of the maximum
470 tensile strength of the reference FF reinforced composite. Figure 8b shows that the maximum tensile

strength evolves linearly with particle aspect ratio in the composite, highlighting the close relationship between particle morphology and composite tensile strength. Therefore, flax shives have an effective reinforcing potential in PP-MAPP composites and cannot be considered as simply 'fillers' since both the modulus and maximum tensile strength are enhanced compared to the sole matrix.

A comparative graph is shown Figure 9, presenting the mechanical properties of injected polypropylene composites manufactured with a similar process involving an equivalent twin-screw extruder. As mentioned previously, the use of fines obtained either from flax fibres or flax shives (FS-50) increases composite stiffness in a similar manner with a slight advantage for FS-50 which increases composite strength at break by 14%. Wood flour and FS-250 have analogue Young's modulus between 2.8 GPa and 2.9 GPa respectively. Our values of flax fibre reinforced injected composites are in agreement with previous work from the literature.

3.2.3 Role of volume fraction on composite properties

Since FS-500 provides the most efficient mechanical properties among the different shive reinforced batches, it was chosen to investigate the influence of volume fractions on composite mechanical properties. Figure 10 represents the evolution of both the maximum tensile strength and the composite's Young modulus as a function of the volume fraction of FS-500. Young's modulus increases linearly with increasing volume fraction (linear fit with $R^2 = 0.94$), highlighting their reinforcing potential. Furthermore, the maximum tensile strength increases with increasing volume fraction up to about 23%-vol of FS-500 and then decreases above this volume fraction. This behaviour is similar to that of other plant cell wall reinforcing materials, such as flax fibres for which the optimum tensile strength in PP-MAPP injection moulded composites is situated at an optimum volume fraction around 33% [20]. We hypotheses that above this volume fraction, particles become too short to effectively reinforce de polymer matrix, presumably due to increasing shear rates induced by particle-particle friction during processing [61].

The fibre aspect ratio decreases during processing with increasing fibre volume fraction due to increasing induced shear rates [59]. In our case, FS-500 aspect ratio after processing is only 4.8 for the 23%-vol fraction against approximately 20 for the flax fibres used in the study of Ausias et al. [20] for a comparable 20% fibre volume fraction; keeping in mind that in their study the initial fibre length

was of 2 mm and that only one step of single-screw extrusion was carried out prior to injection moulding; and this manufacturing process causes fibres to be randomly dispersed in the samples.

3.2.4 Analysis of the critical aspect ratio

When considering a unidirectional composite reinforced by short fibres assumed to be parallel to the applied stress, fibre aspect ratio will influence its tensile strength at break [62]. Assuming that i) the applied load must be transferred to the fibre by the fibre-matrix interface, ii) no loads are transferred at the fibre's section, iii) shear stresses are constant along the fibre's length, iv) the matrix's strain at break is considerably higher than that of the fibres, v) both the matrix and the reinforcing fibres have an elastic and linear behaviour, and vi) the fibres are solid cylinders, Kelly and Tyson established a simplified model [63] defining the critical fibre length L_c as follows (Eq. 3) :

$$L_c = \frac{\sigma_{f,u}\, d}{2\,\tau_i} \qquad \text{Eq. 3}$$

Where $\sigma_{f,u}$ is the ultimate fibre stress, d the fibre diameter and τ_i is shear stress at the fibre-matrix interface. The calculation details can be found in different composite literature, by Gibson for instance [62]. The critical aspect ratio can then be considered as the minimal aspect ratio for a fibre to break without pull-out.

SEM images of the fracture surface of PP-MAPP and FS-500 composites (Figure 11) shows that some large particles maintain their alveolar cell structure even after processing, and that the matrix is able to penetrate in it. Furthermore, it even appears that in some places rupture takes place through the flax shive particles due to matrix infiltration (Fig. 11b).

Let us consider FS as a tubular structure in which the elementary volumes, immersed in matrix, have a central lumen completely impregnated by the polymer, as shown in Figure 11b. FS can be simplified as a hollow cylinder having a length L, an average diameter $\bar{d}_f$ and a thickness e. In a similar reasoning as previous, tubes are considered to be parallel to one another in a unidirectional composite. Let's consider d_x, an infinitely small portion of this hollow cylinder along the x axis being fully impregnated with the polymer matrix (as shown in Figure 12), and that the cylinder is parallel to a tensile solicitation of the composite. If we consider, as did Kelly and Tyson, that reinforcing is done in the form of shear stresses considered to be constant along cylinder's length, then the forces applied to the cylinder can be summarized as follows (Eq. 4):

$$(\sigma_{cw} + d\sigma_{cw})S = \sigma_{cw}S + \tau_{i,ins}\left(\bar{d}_f + e\right)d_x + \tau_{i,ext}\left(\bar{d}_f - e\right)d_x \qquad \text{Eq. 4}$$

With $\sigma_{cw}$the tensile strength applied to the cylinder's surface *S*, τ_e the shear stresses applied on its external surface and τ_i those applied to its inside.

Since the matrix is considered to have an elastic behaviour, then $\tau_{i,ins} = \tau_{i,ext}$, and when resolving this equation based on the Kelly-Tyson model by integration along the cylinder's length, then the previous equation (Eq.4) becomes equation 5, and the critical length at which tensile strength causes cell wall rupture does not depend on fibre diameter (as previously established in equation 3), but rather on the cell wall thickness.

$$L_c = \frac{\sigma_{cw,u} * e}{\tau_i} \qquad \text{Eq. 5}$$

To the best of our knowledge, the average flax xylem cell wall tensile strength has not been reported in the literature. If we consider that flax shives are mainly made of secondary xylem with a composition and structure similar to that of wood, then we can assume that the tensile yield strength of the cell walls of flax shives is also similar to that of gymnosperm earlywood which was measured to be 350 MPa for *Pinus Radiata* [64]. In ongoing studies, we measured the global cell wall thickness in flax xylem to be of 2.4 µm on average by SEM observations of a stem's transverse section. Merotte et al. [65] measured an interfacial shear strength (IFSS) between flax and MAPP of 10.6 ± 2.8 MPa. Therefore, the critical length of a tubular structure assimilated to FS is estimated to be about 79 µm (Eq. 5); against 526 µm estimated using the Kelly-Tyson model (Eq. 3) for a solid-section flax fibre of 15 µm in diameter and an ultimate strength at break of 950 MPa [66]. This is a 6.7 times lower critical length when using this simplistic model, showing the potential reinforcing efficiency of particles which may be considered as fines (less than 200 µm in length) but having a hollow structure, due to the importance of cell wall thickness rather than aspect ratio.

Clearly, in this simplified model the lumen is considered to fully impregnated, and cell wall orientation, matrix wetting and cell wall-matrix adhesion are just a few parameters that might influence shear stresses inside and outside of the tubular cell wall, which may therefore not be equal in reality. Furthermore, cell wall thickness in the xylem evolves with cell wall type, plant maturity and along a flax stem, whereas FS are an assembly of all these different elements creating a gradient in reinforcing potential. Additionally, the assumption that cells are circular is preferred for estimation purposes, but cell wall most often have a polygonal transversal shape that should also be accounted for. This makes FS fragmentation a determining factor for hollow cell accessibility by the matrix.

4. Conclusion

This study focused on the reinforcement potential of flax shives in PP-MAPP injection moulded composites following the investigation of the fragmented by-product materials. The granulometry analysis succeeding raw FS comminution highlights the importance of the mode of particle size analysis which can easily hide small particles or fines. The volume distribution of fragmented flax shives shows that the FS-250 and FS-500 batches are comprised of a high number of particles having a well conserved alveolar structure. Due to the nature of cells, FS have a different biochemical composition than flax fibres as the former contain less than half the latter's amount of cellulose and around six times the latter's amount of lignin. The composition of FS does not evolve with fragmentation, even after an intense attrition-beads milling process. However, the crystallinity index of FS decreases with comminution up to a 50% for the severely transformed FS-50 due to amorphization of particles resulting in a decrease in degree of polymerization and therefore sample crystallinity, as well as a conversion of crystalline cellulose I into cellulose II or III.

Following this preliminary study, the tensile mechanical properties of injection moulded PP-MAPP composites were evaluated. Compounding and injection moulding induced a 70% decrease in flax fibre and FS-250 length but did not modify the length of FS-50 due to their initially small particle size. The tensile maximum strength of the composites increases linearly with particle aspect ratio, and interestingly, FS-500 tensile Young's modulus reaches 90% that of the reference FF composite. The FS-500 sample presented the best mechanical properties among the other fragmented FS batches and was chosen to further analyse the consequences of FS volume fraction. Unlike flax fibres, FS-500 present an optimal tensile strength at 23% in volume fraction, against 33%-vol for flax fibres. SEM observations reveal that the matrix is able to penetrate in some flax shives having a tubular structure. In the case of a hollow cylinder fully impregnated by the matrix, we have shown that the critical length of the particle depends not on particle diameter but rather on tube wall thickness, highlighting the reinforcing potential of hollow fines. The study shows the legitimacy of flax shives as reinforcing material in the field of biocomposites.

5. Acknowledgments

The authors would like to thank the National Association of Research and Technology for financing a thesis in partnership with Van Robaeys Frères and the Dupuy de Lôme Research Institute of the South Brittany University (France). Furthermore, authors would like to thank Gwendoline Guillouroux and Maelenn le Gall from IFREMER for their valuable work, as well as Sylviane Daniel from INRA for her kindness with biochemical analysis and Philippe Violle from Sympatec for his availability and good guidance on the project.

References:

[1] J. Beaugrand, M. Nottez, J. Konnerth, and A. Bourmaud, “Multi-scale analysis of the structure and mechanical performance of woody hemp core and the dependence on the sampling location,” *Ind. Crops Prod.*, vol. 60, pp. 193–204, 2014.

[2] T. Väisänen, A. Haapala, R. Lappalainen, and L. Tomppo, “Utilization of agricultural and forest industry waste and residues in natural fiber-polymer composites : A review,” *Waste Manag.*, vol. 54, pp. 62–73, 2016.

[3] A. O. Ogah and J. N. Afiukwa, “Characterization and comparison of mechanical behavior of agro fiber-filled high-density polyethylene bio-composites,” *J. Reinf. Plast. Compos.*, vol. 33, pp. 37–46, 2014.

[4] A. Le Duigou, J. M. Deux, P. Davies, and C. Baley, “PLLA/flax mat/balsa bio-sandwich-environmental impact and simplified life cycle analysis,” *Appl. Compos. Mater.*, vol. 19, no. 3–4, pp. 363–378, 2012.

[5] M. Pervaiz and M. M. Sain, “Carbon storage potential in natural fiber composites,” *Resour. Conserv. Recycl.*, vol. 39, no. 4, pp. 325–340, 2003.

[6] S. Réquilé, C. Goudenhooft, A. Bourmaud, A. Le Duigou, and C. Baley, “Exploring the link between flexural behaviour of hemp and flax stems and fibre stiffness,” *Ind. Crops Prod.*, vol. 113, no. January, pp. 179–186, 2018.

[7] F. Bert, “Lin fibre: Culture et transformation,” *Arvalis-Institut du Végétal Paris, Fr.*, 2013.

[8] J. Foulk, D. E. Akin, R. Dodd, and C. Ulven, “Production of Flax Fibers for Biocomposites,” in *Cellulose Fibers: Bio- and Nano-Polymer Composites*, Berlin, Heidelberg: Springer Berlin Heidelberg, 2011, pp. 61–95.

[9] W. E. Marshall, L. H. Wartelle, and D. E. Akin, “Flax shive as a source of activated carbon for metals remediation,” *BioResources*, vol. 2, pp. 82–90, 2007.

[10] V. Dubois, A. Leblanc, O. Carpentier, G. Alhaik, and E. Wirquin, “Performances of flax shive-based lightweight composites with rapid hardening,” *Constr. Build. Mater.*, vol. 165, pp. 17–27, 2018.

[11] S. González-García, L. Luo, M. T. Moreira, G. Feijoo, and G. Huppes, “Life cycle assessment of flax shives derived second generation ethanol fueled automobiles in Spain,” *Renew. Sustain. Energy Rev.*, vol. 13, no. 8, pp. 1922–1933, Oct. 2009.

[12] C. Goudenhooft, A. Bourmaud, and C. Baley, “Varietal selection of flax over time: Evolution of plant architecture related to influence on the mechanical properties of fibers,” *Ind. Crops Prod.*, vol. 97, pp. 56–64, 2017.

[13] W. Hu, M. Zhang, M. T. Ton-That, and T. dung Ngo, “A comparison of flax shive and extracted flax shive reinforced PP composites,” *Fibers Polym.*, vol. 15, no. 8, pp. 1722–1728, 2014.

[14] A. Day *et al.*, “Lignification in the flax stem: Evidence for an unusual lignin in bast fibers,” *Planta*, vol. 222, no. 2, pp. 234–245, 2005.

[15] N. Chevanan, A. R. Womac, V. S. Bitra, and S. Sokhansanj, “Effect of Particle Size Distribution on Loose-filled and Tapped Densities of Selected Biomass after Knife Mill Size Reduction,” *Appl. Eng. Agric.*, vol. 27, no. 4, pp. 631–644, 2011.

[16] C. Mayer-Laigle, R. Rajaonarivony, N. Blanc, and X. Rouau, “Comminution of Dry Lignocellulosic Biomass: Part II. Technologies, Improvement of Milling Performances, and Security Issues,” *Bioengineering*, vol. 5, no. 3, p. 50, 2018.

[17] J. A. Howsmon and R. H. Marchessault, “The ball-milling of cellulose fibers and recrystallization effects,” *J. Appl. Polym. Sci.*, vol. 1, no. 3, pp. 313–322, May 1959.

[18] T. Qiang, J. Wang, and M. P. Wolcott, “Facile Preparation of Cellulose/Polylactide Composite Materials with Tunable Mechanical Properties,” *Polym. - Plast. Technol. Eng.*, vol. 57, no. 13, pp. 1288–1295, 2018.

[19] A. K. Bledzki, A. A. Mamun, and O. Faruk, “Abaca fibre reinforced PP composites and comparison with jute and flax fibre PP composites,” *Express Polym. Lett.*, vol. 1, no. 11, pp. 755–762, 2007.

[20] G. Ausias, A. Bourmaud, G. Coroller, and C. Baley, “Study of the fibre morphology stability in polypropylene-flax composites,” *Polym. Degrad. Stab.*, vol. 98, no. 6, pp. 1216–1224, 2013.

[21] A. Bourmaud, A. Le Duigou, and C. Baley, “Mechanical performance of flax-based biocomposites,” in *Biocomposites*, Fourteenth., Elsevier Ltd., 2015, pp. 365–399.

[22] M. Tanguy, A. Bourmaud, J. Beaugrand, T. Gaudry, and C. Baley, “Polypropylene reinforcement with flax or jute fibre; Influence of microstructure and constituents properties on the performance of composite,” *Compos. Part B Eng.*, vol. 139, no. November 2016, pp. 64–74, 2018.

[23] N. Graupner, G. Ziegmann, F. Wilde, F. Beckmann, and J. Müssig, “Procedural influences on

compression and injection moulded cellulose fibre-reinforced polylactide (PLA) composites: Influence of fibre loading, fibre length, fibre orientation and voids," *Compos. Part A Appl. Sci. Manuf.*, vol. 81, pp. 158–171, 2016.

[24] A. Bourmaud, G. Ausias, G. Lebrun, M. Tachon, and C. Baley, "Observation of the structure of a composite polypropylene / flax and damage mechanisms under stress," *Ind. Crop. Prod.*, vol. 43, pp. 225–236, 2013.

[25] N. M. Stark and R. E. Rowlands, "Effects of wood fiber characteristics on mechanical properties of wood/polypropylene composites," *Wood fiber Sci. Vol. 35, no. 2 Pages 167-174*, 2003.

[26] K. Albrecht, T. Osswald, E. Baur, T. Meier, S. Wartzack, and J. Müssig, "Fibre Length Reduction in Natural Fibre-Reinforced Polymers during Compounding and Injection Moulding—Experiments Versus Numerical Prediction of Fibre Breakage," *J. Compos. Sci.*, vol. 2, no. 2, p. 20, Mar. 2018.

[27] N. Martin, N. Mouret, P. Davies, and C. Baley, "Influence of the degree of retting of flax fibers on the tensile properties of single fibers and short fiber/polypropylene composites," *Ind. Crops Prod.*, vol. 49, pp. 755–767, 2013.

[28] M. H. B. Snijder and H. L. Bos, "Reinforcement of polypropylene by annual plant fibers: Optimisation of the coupling agent efficiency," *Compos. Interfaces*, vol. 7, no. 2, pp. 69–75, 2000.

[29] G. Coroller, "Contribution à l'étude des matériaux composites renforcés par des fibres végétales: cas des composites extrudés à matrice polypropylène," Lorient, 2013.

[30] C. Mayer-Laigle, N. Blanc, R. Rajaonarivony, and X. Rouau, "Comminution of Dry Lignocellulosic Biomass, a Review: Part I. From Fundamental Mechanisms to Milling Behaviour," *Bioengineering*, vol. 5, no. 2, p. 41, 2018.

[31] J. F. Thibault, "Automatisation du dosage des substances pectiques par la methode au meta-hydroxydiphenyl," *Lebensmittel - Wissenschaft + Technologie. Food science + technology*, vol. v. 12. 1979.

[32] A. B. Blakeney, P. J. Harris, R. J. Henry, and B. A. Stone, "A simple and rapid preparation of alditol acetates for monosaccharide analysis," *Carbohydr. Res.*, vol. 113, no. 2, pp. 291–299, Mar. 1983.

[33] R. Hatfield and R. S. Fukushima, “Can lignin be accurately measured?,” *Crop Sci.*, vol. 45, no. 3, pp. 832–839, 2005.

[34] L. Segal, J. J. Creely, A. E. Martin, and C. M. Conrad, “An Empirical Method for Estimating the Degree of Crystallinity of Native Cellulose Using the X-Ray Diffractometer,” *Text. Res. J.*, vol. 29, no. 10, pp. 786–794, Oct. 1959.

[35] S. Park, J. O. Baker, M. E. Himmel, P. A. Parilla, and D. K. Johnson, “Cellulose crystallinity index: measurement techniques and their impact on interpreting cellulase performance,” *Biotechnol. Biofuels*, vol. 3, no. 1, p. 10, 2010.

[36] M. Le Gall, P. Davies, N. Martin, and C. Baley, “Recommended flax fibre density values for composite property predictions,” *Ind. Crops Prod.*, vol. 114, no. February, pp. 52–58, 2018.

[37] N. Le Moigne, M. Van Den Oever, and T. Budtova, “A statistical analysis of fibre size and shape distribution after compounding in composites reinforced by natural fibres,” *Compos. Part A*, vol. 42, no. 10, pp. 1542–1550, 2011.

[38] L. Teuber, H. Militz, and A. Krause, “Dynamic particle analysis for the evaluation of particle degradation during compounding of wood plastic composites,” *Compos. Part A Appl. Sci. Manuf.*, vol. 84, pp. 464–471, 2016.

[39] K. Haag and J. Müssig, “Scatter in tensile properties of flax fibre bundles : influence of determination and calculation of the cross- sectional area,” *J. Mater. Sci.*, vol. 51, pp. 7907–7917, 2016.

[40] E. Di Giuseppe *et al.*, “Reliability evaluation of automated analysis, 2D scanner, and micro-tomography methods for measuring fiber dimensions in polymer-lignocellulosic fiber composites,” *Compos. Part A Appl. Sci. Manuf.*, vol. 90, pp. 320–329, Nov. 2016.

[41] A. Bourmaud, C. Mayer-Laigle, C. Baley, and J. Beaugrand, “About the frontier between filling and reinforcement by fine flax particles in plant fibre composites,” *Ind. Crops Prod.*, vol. 141, no. September, p. 111774, Dec. 2019.

[42] P. Evon *et al.*, “Production of fiberboards from shives collected after continuous fiber mechanical extraction from oleaginous flax,” *J. Nat. Fibers*, vol. 00, no. 00, pp. 1–17, Jan. 2018.

[43] C. Goudenhooft, “Multi-scale characterization of flax stems and fibers : structure and mechanical performances,” 2018.

[44] P. Trivelato, C. Mayer, A. Barakat, H. Fulcrand, and C. Aouf, “Douglas bark dry fractionation for polyphenols isolation : From forestry waste to added value products,” *Ind. Crop. Prod.*, vol. 86, pp. 12–15, 2016.

[45] A. U. Buranov, K. A. Ross, and G. Mazza, “Isolation and characterization of lignins extracted from flax shives using pressurized aqueous ethanol,” *Bioresour. Technol.*, vol. 101, no. 19, pp. 7446–7455, 2010.

[46] T. A. Gorshkova *et al.*, “Specific type of secondary cell wall formed by plant fibers,” *Russ. J. Plant Physiol.*, vol. 57, no. 3, pp. 328–341, 2010.

[47] G. Değer, M. Pakdemirli, F. Candan, S. Akgün, and H. Boyacı, “Strength of Wheat and Barley Stems and Design of New Beam/Columns,” *Math. Comput. Appl.*, vol. 15, no. 1, pp. 1–13, Apr. 2010.

[48] R. C. Pettersen, “The chemical composition of wood,” in *The chemistry of solid wood*, CRC Press, 1985, pp. 57–126.

[49] A. D. French, “Idealized powder diffraction patterns for cellulose polymorphs,” *Cellulose*, vol. 21, no. 2, pp. 885–896, 2014.

[50] A. S. Khan *et al.*, “Impact of Ball-Milling Pretreatment on Pyrolysis Behavior and Kinetics of Crystalline Cellulose,” *Waste and Biomass Valorization*, vol. 7, no. 3, pp. 571–581, 2015.

[51] C. M. Lee *et al.*, “Cellulose polymorphism study with sum-frequency-generation (SFG) vibration spectroscopy: identification of exocyclic CH2OH conformation and chain orientation,” *Cellulose*, vol. 20, no. 3, pp. 991–1000, Jun. 2013.

[52] Z. Tang *et al.*, “TEMPO-Oxidized cellulose with high degree of oxidation,” *Polymers (Basel).*, vol. 9, no. 9, pp. 3–4, 2017.

[53] C. C. Piras, S. Fernández-Prieto, and W. M. De Borggraeve, “Ball milling: a green technology for the preparation and functionalisation of nanocellulose derivatives,” *Nanoscale Adv.*, pp. 937–947, 2019.

[54] L. Y. Yatsu, T. A. Calamari, and R. R. Benerito, “Conversion of Cellulose I to Stable Cellulose III,” *Text. Res. J.*, vol. 56, no. 7, pp. 419–424, 1986.

[55] M. Ago, T. Endo, and T. Hirotsu, “Crystalline transformation of native cellulose from cellulose I to cellulose II polymorph by a ball-milling method with a specific amount of water,” *Cellulose*, vol. 11, no. 2, pp. 163–167, 2004.

[56] V. Kocherbitov, S. Ulvenlund, M. Kober, K. Jarring, and T. Arnebran, “Hydration of microcrystalline cellulose and milled cellulose studied by sorption calorimetry,” *J. Phys. Chem. B*, vol. 112, no. 12, pp. 3728–3734, 2008.

[57] S. T. Su, J. Xiong, and J. Ye, “Effect of Ball Milling on Structure of Microcrystalline Cellulose,” *Appl. Mech. Mater.*, vol. 394, pp. 201–204, 2013.

[58] X. H. Liang, L. Z. Gu, and E. Y. Ding, “Recrystallization behavior of cellulose and lignocellulose from Pinus massoniana,” *Wood Sci. Technol.*, vol. 27, no. 6, pp. 461–467, 1993.

[59] A. Le Duc, B. Vergnes, and T. Budtova, “Polypropylene/natural fibres composites: Analysis of fibre dimensions after compounding and observations of fibre rupture by rheo-optics,” *Compos. Part A Appl. Sci. Manuf.*, vol. 42, no. 11, pp. 1727–1737, 2011.

[60] C. Gourier, A. Bourmaud, A. Le Duigou, and C. Baley, “Influence of PA11 and PP thermoplastic polymers on recycling stability of unidirectional flax fibre reinforced biocomposites,” *Polym. Degrad. Stab.*, vol. 136, pp. 1–9, 2017.

[61] D. M. Bigg, D. F. Hiscock, J. R. Preston, and E. J. Bradbury, “Thermoplastic matrix sheet composites,” *Polym. Compos.*, vol. 9, no. 3, pp. 222–228, Jun. 1988.

[62] R. F. Gibson, *Principles of Composite Material Mechanics*. 1994.

[63] A. Kelly and W. R. Tyson, “Tensile Properties of Fibre-Reinforced Metals: Copper/Tungsten and Copper/Molybdenum,” *J. Mech. Phys. Solids*, vol. 13, pp. 329–350, 1965.

[64] I. D. Cave, “The longitudinal Young’s modulus of Pinus radiata,” *Wood Sci. Technol.*, vol. 3, no. 1, pp. 40–48, 1969.

[65] J. Merotte *et al.*, “Flax and hemp nonwoven composites : The contribution of interfacial bonding to improving tensile properties,” *Polym. Test.*, vol. 66, pp. 303–311, 2018.

[66] C. Baley and A. Bourmaud, “Average tensile properties of French elementary flax fibers,” *Mater. Lett.*, vol. 122, pp. 159–161, 2014.

FIGURE CAPTIONS

Figure 1. Reinforcing material length distribution after comminution a) in number, b) in volume. The 10^{th} (first decile), 16^{th}, 50^{th} (median), 84^{th}, and 90^{th} (last decile) percentiles of the cumulative distribution in length are shown respectively from bottom up with corresponding values of 16^{th}, 50^{th} and 84^{th} percentiles facing them.

Figure 2. Length distribution of reinforcing materials and visual aspect as observed with SEM.

Figure 3. Preserved cell wall alveolar structure of some FS-250 particles after comminution. Arrow points to an interesting tracheary element of the flax xylem.

Figure 4. Analysis of lignin, glucose and non-glucosidic monosaccharide content of reinforcing materials.

Figure 5. a) XRD spectra for the ball milled flax shives (raw, 50, 250, 500). For reference, the XRD spectra of Avicel cellulose from Lee et al. [49] marked with * on the graph are also illustrated. b) The evolution in the crystallinity of the samples.

Figure 6. a) Particle length distribution in volume and b) Aspect ratios of extracted materials. The 10th (first decile), 16th, 50th (median), 84th, and 90th (last decile) percentiles of the cumulative distribution in length are shown respectively from bottom up with the 16th, 50th and 84th percentile values facing them.

Figure 7. Screw design of the twin screws used for extrusion, with both transportation areas (white) and kneading areas (grey). Screw length L/D is 40, flow direction is from right to left.

Figure 8. a) Typical tensile stress and deformation behaviour of 30%-wt reinforced PP-MAPP composites, b) Maximum tensile strength of PP-MAPP reinforced composite as function of reinforcing material aspect ratio.

Figure 9. Comparison of mechanical properties provided by different reinforcing materials. For all the batches of this study, both PP-MAPP matrix and extrusion machine are the same. Samples marked with * are obtained from [40].

Figure 10. The Young's modulus and maximum tensile strength of FS-500 reinforced composite as function of volume fraction.

Figure 11. a) Fracture surface of the FS-500 reinforced PP-MAPP composite b) Highlight of a potential matrix penetration in the alveolar structure. Arrows indicate cell-walls.

Figure 12. Schematic representation of the mechanical forces applied to a hollow tubular short cell wall structure in a polymer matrix during tensile testing.

TABLE CAPTIONS

Table 1. Reinforcing material samples and corresponding abbreviations.

Table 2. Tensile properties of injected composites reinforced with 30%-wt reinforcing materials.

Color should be used for all figures in manuscript.

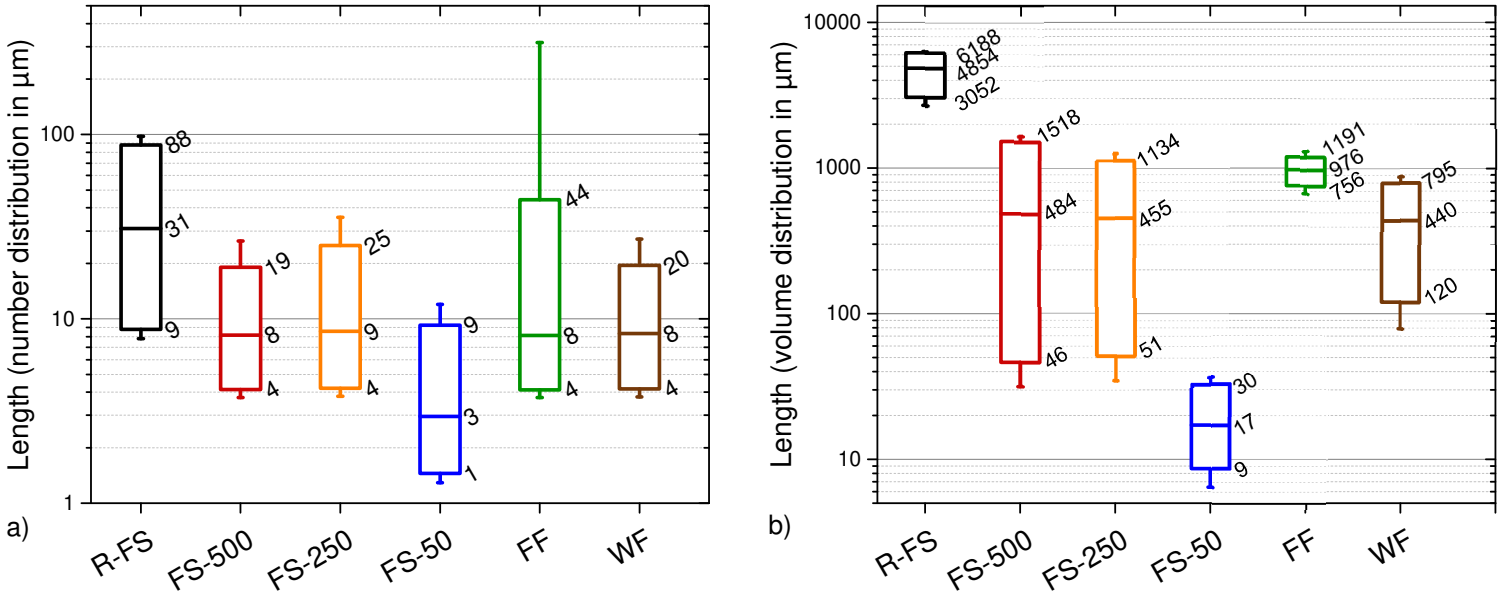

Figure 1. Reinforcing material length distribution after comminution a) in number, b) in volume. The 10th (first decile), 16th, 50th (median), 84th, and 90th (last decile) percentiles of the cumulative distribution in length are shown respectively from bottom up with corresponding values of 16th, 50th and 84th percentiles facing them.

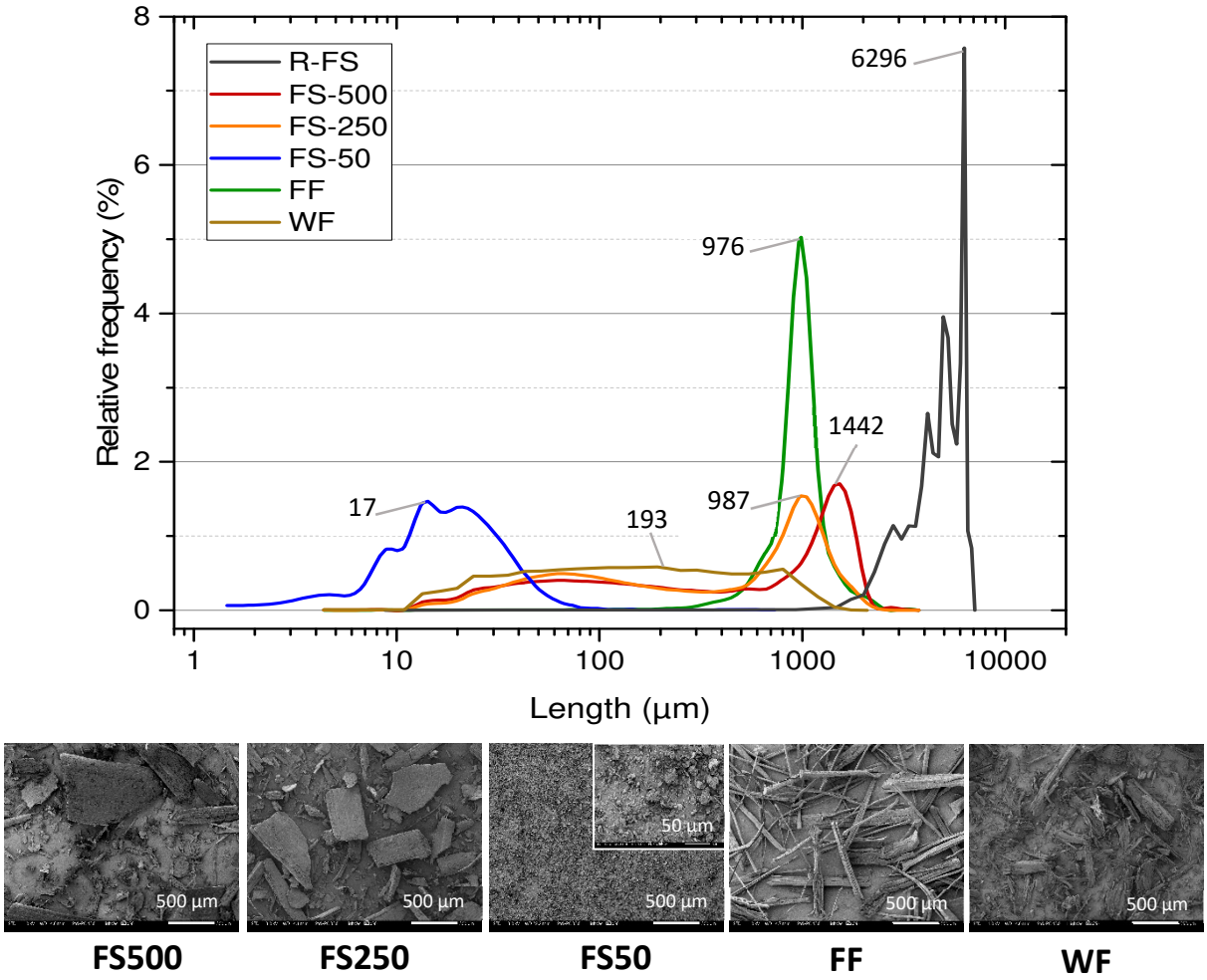

Figure 2. Length distribution of reinforcing materials and visual aspect as observed with SEM.

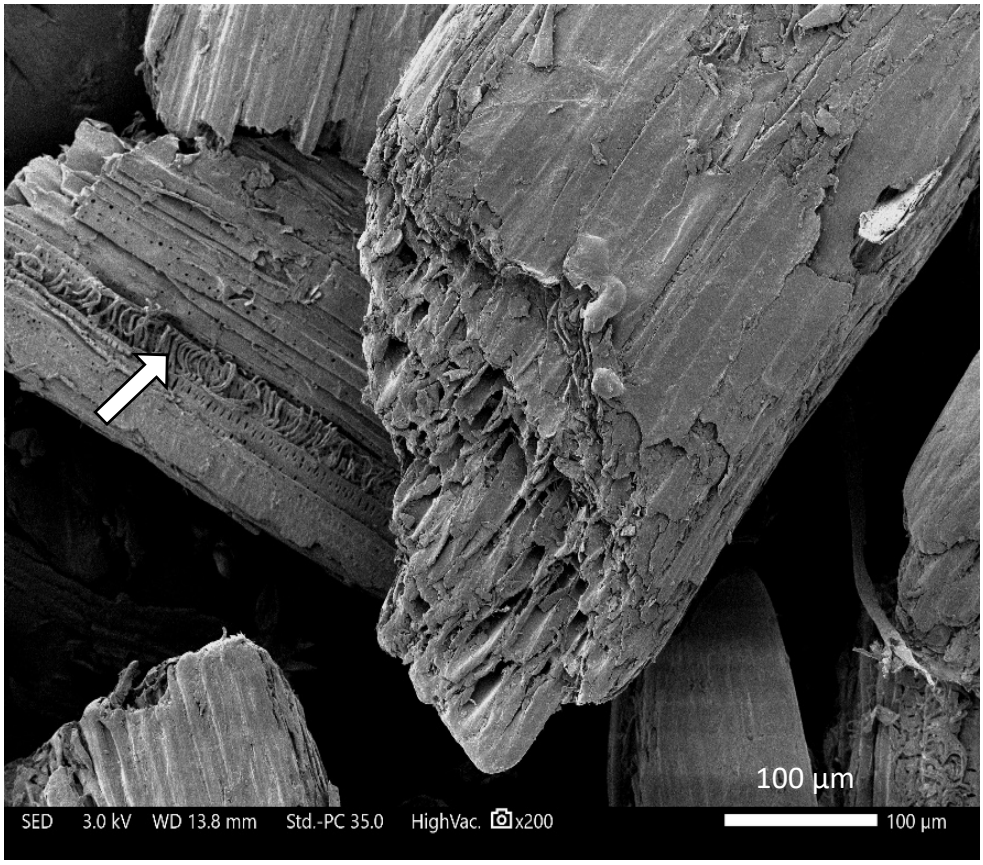

Figure 3. Preserved cell wall alveolar structure of some FS-250 particles after comminution. Arrow points to an interesting tracheary element of the flax xylem.

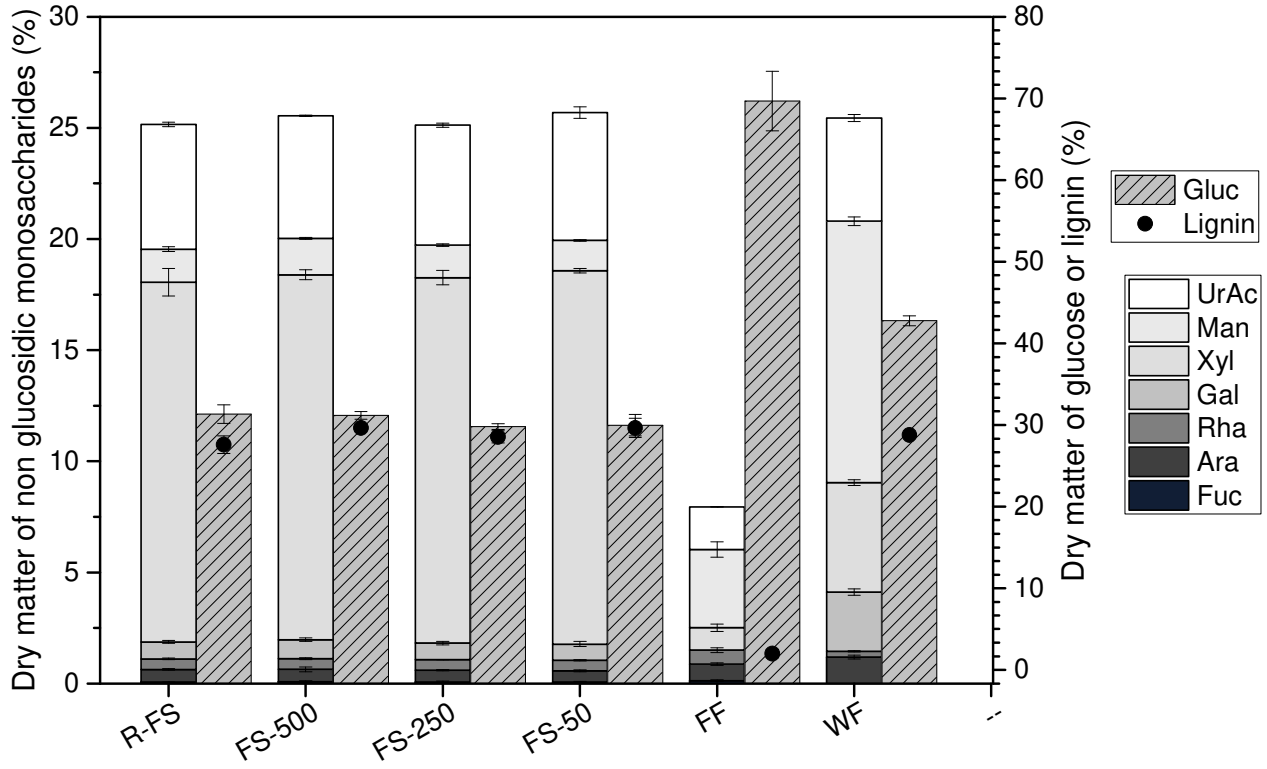

Figure 4. Analysis of lignin, glucose and non-glucosidic monosaccharide content of reinforcing materials.

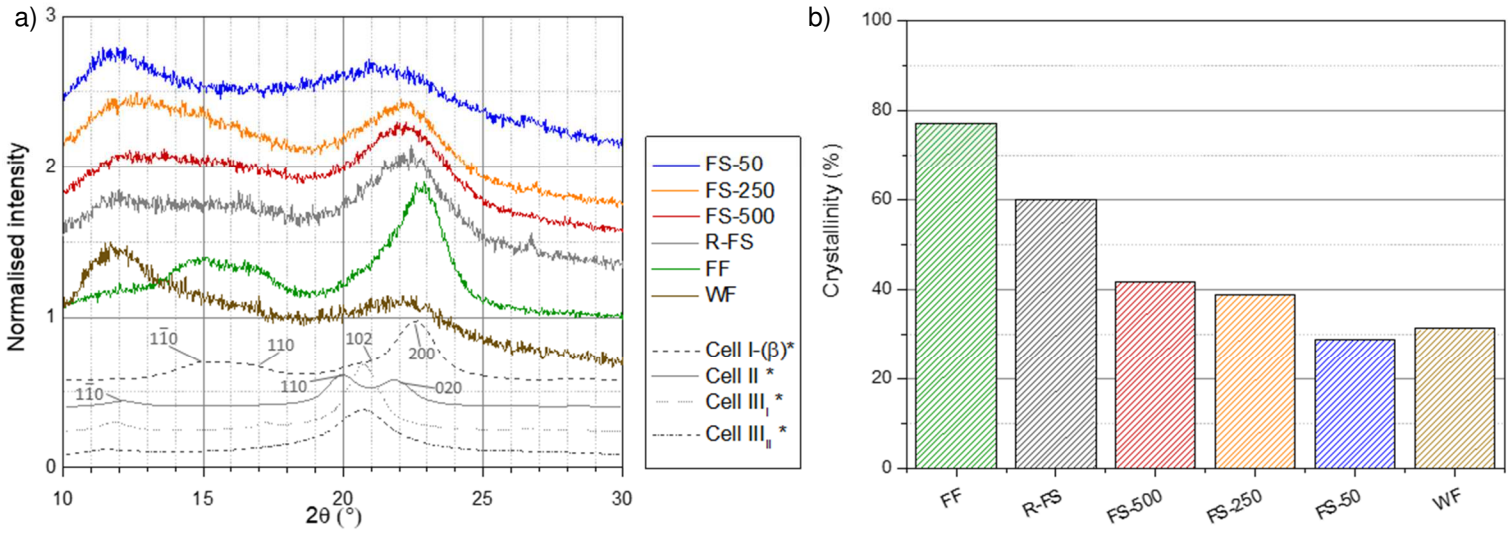

*Figure 5. a) XRD spectra for the fragmented flax shives (raw, 50, 250, 500). For reference, the XRD spectra of Avicel cellulose from Lee et al. [49] marked with * on the graph are also illustrated. b) The evolution in the crystallinity of the samples.*

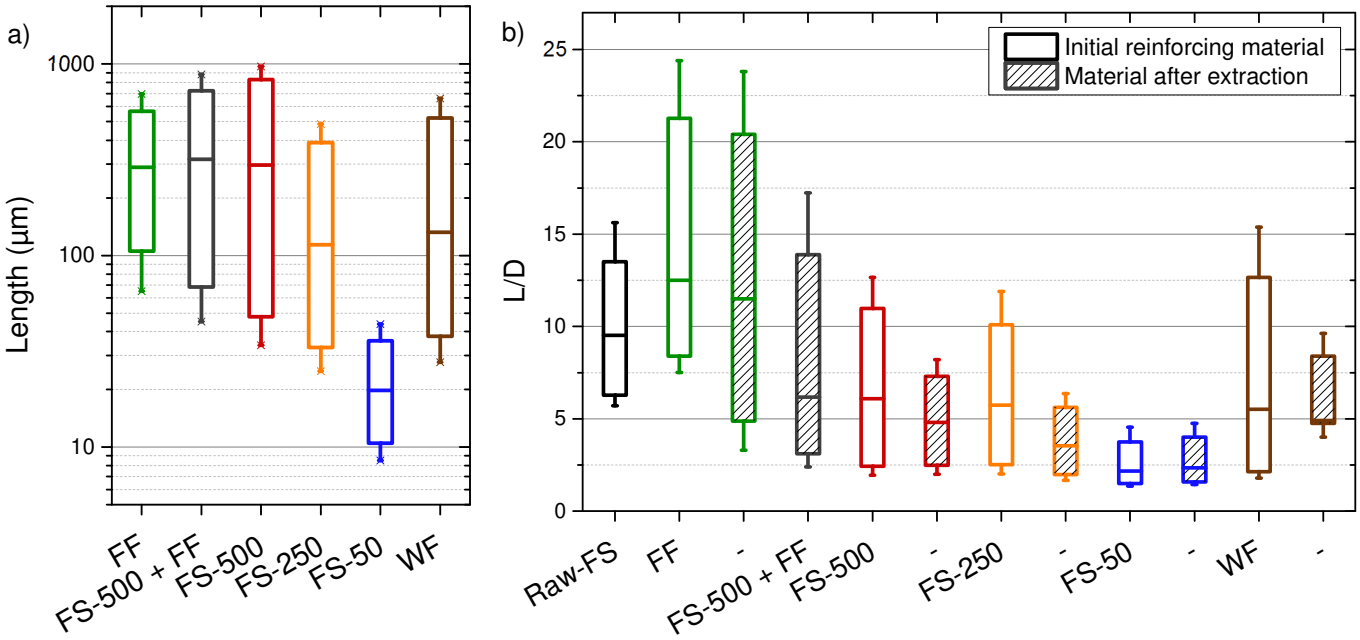

Figure 6. a) Particle length distribution in volume and b) Aspect ratios of initial reinforcing material compared to extracted materials from the 30%-wt reinforced PP-MAPP composite. The 10th (first decile), 16th, 50th (median), 84th, and 90th (last decile) percentiles of the cumulative distribution in length are shown respectively from bottom up.

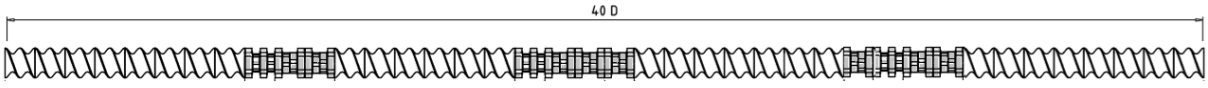

Figure 7. Screw design of the twin screws used for extrusion, with both transportation areas (white) and kneading areas (grey). Screw length L/D is 40, flow direction is from right to left.

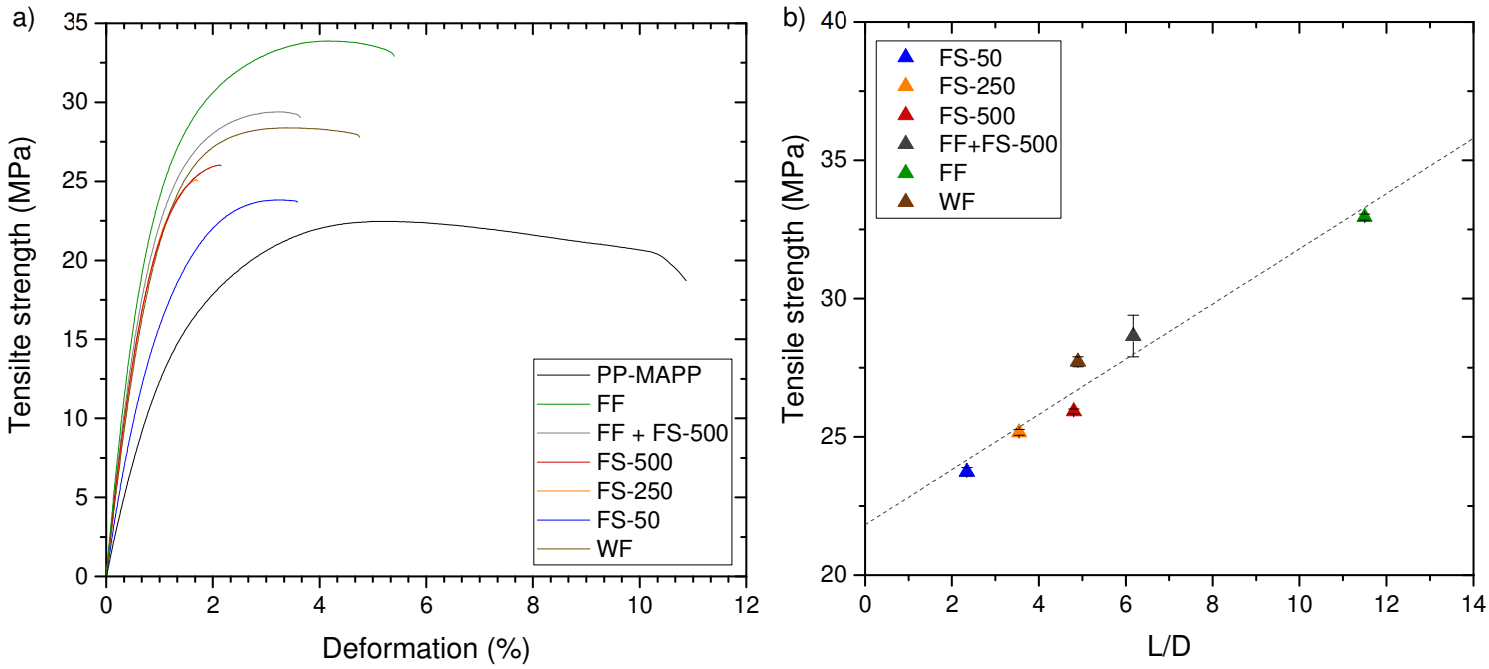

Figure 8. a) Typical tensile stress and deformation behaviour of 30%-wt reinforced PP-MAPP composites, b) Maximum tensile strength of PP-MAPP reinforced composite as function of reinforcing material aspect ratio.

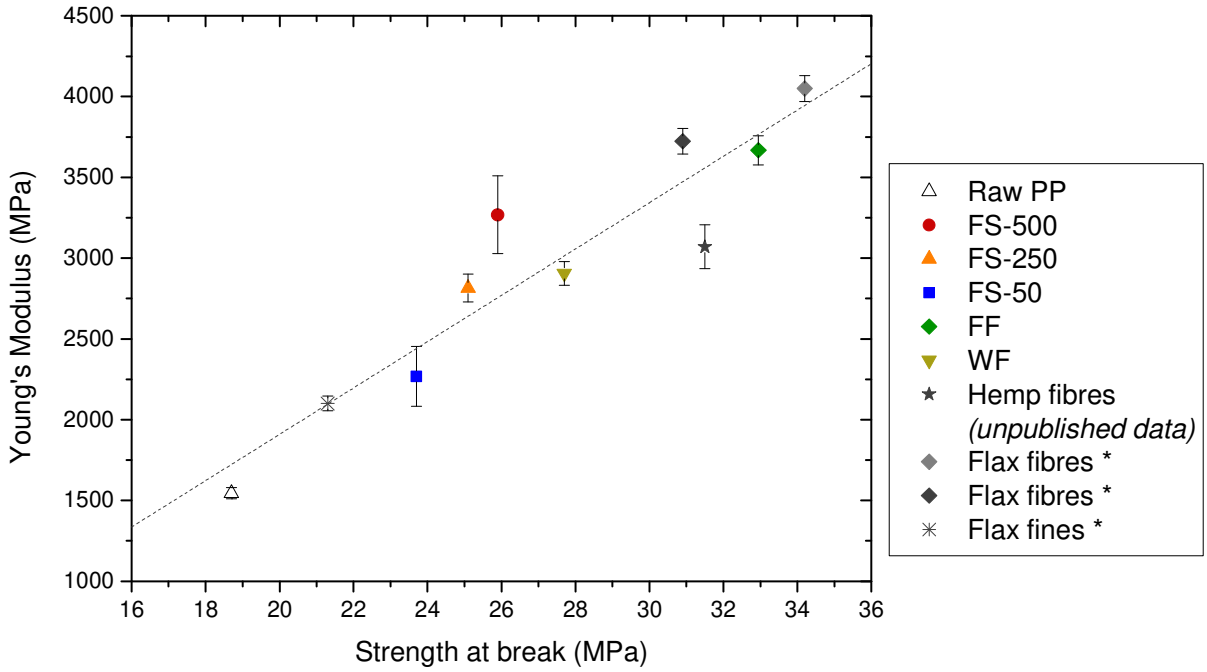

*Figure 9. Comparison of mechanical properties provided by different reinforcing materials. For all the batches of this study, both PP-MAPP matrix and extrusion machine are the same. Samples marked with * are obtained from [40].*

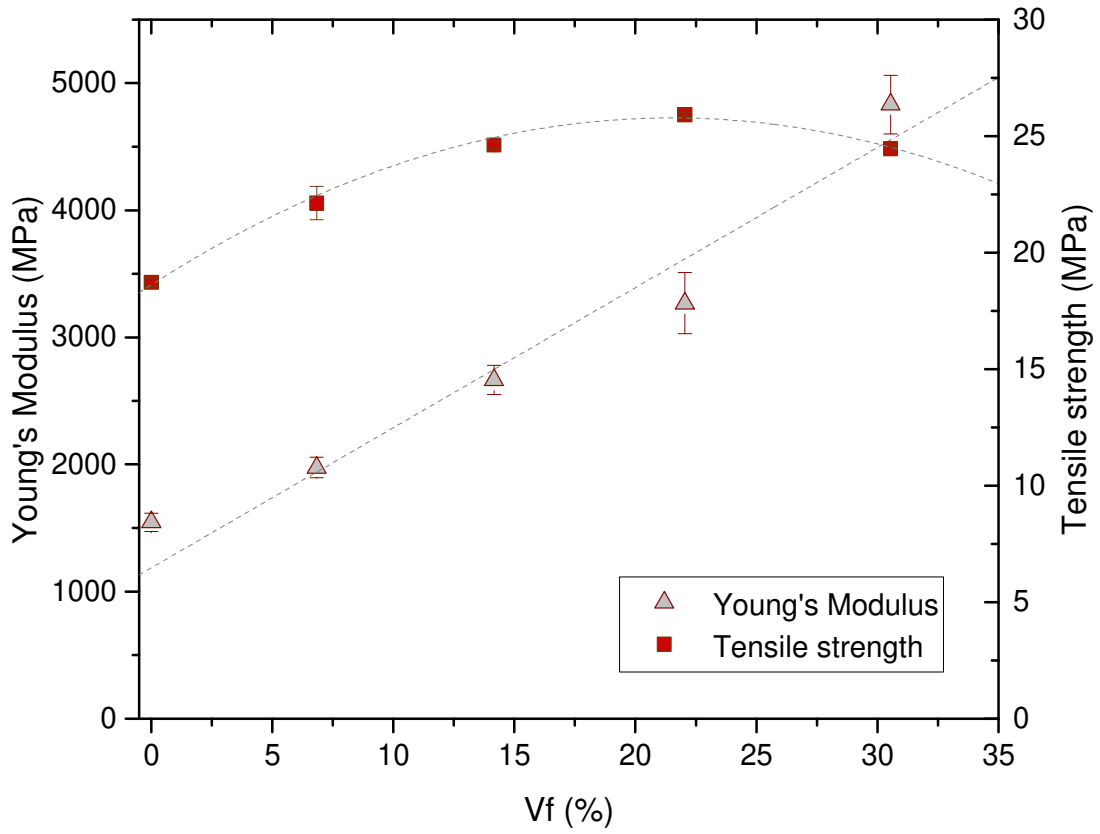

Figure 10. The Young's modulus and maximum tensile strength of FS-500 reinforced composite as function of volume fraction.

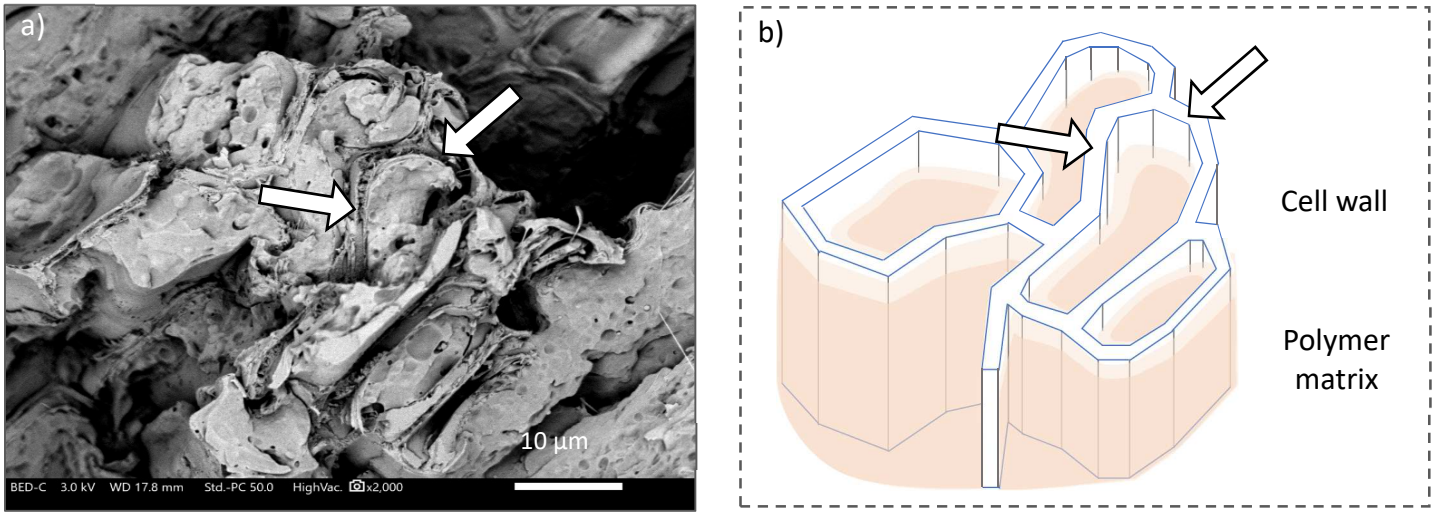

Figure 11. a) SEM observation of the fracture surface of the 30%-wt FS-500 reinforced PP-MAPP composite b) Highlight of a potential matrix penetration in the alveolar structure. Arrows indicate cell-walls.

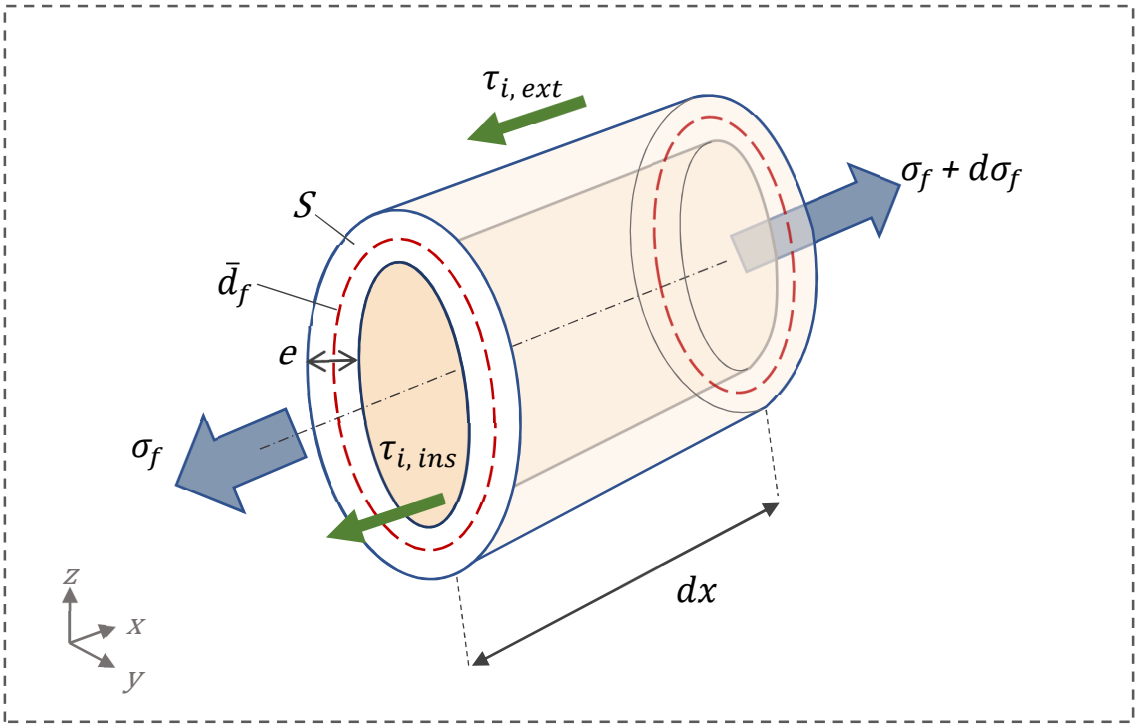

Figure 12. Schematic representation of the mechanical forces applied to a hollow tubular short cell wall structure in a polymer matrix during tensile testing.

Table 1. Reinforcing material samples and corresponding abbreviations.

Sample	**Abbreviation**	**Processing steps**
Raw flax shives	R-FS	Obtained from scutching of flax
Flax shives 50	FS-50	Attrition beads milling of R-FS
Flax shives 250	FS-250	Knife milling of R-FS
Flax shives 500	FS-500	Knife milling of R-FS
Flax fibres and flax shives 500	FF + FS-500	50/50-wt mix of FS-500 and FF
Flax fibres	FF	Scutching, hackling and cutting
Wood flour	WF	Fragmentation and sieving

Table 2. Tensile properties of injected composites reinforced with 30%-wt reinforcing materials.

	Young's Modulus *(MPa)*	**Maximum tensile strength** *(MPa)*	**Ultimate strain** *(%)*
PP-MAPP	1545 (± 076)	18.7 (± 0.2)	10.9 (± 0.3)
FS-50	2269 (± 185)	23.7 (± 0.2)	3.4 (± 0.4)
FS-250	2815 (± 086)	25.2 (± 0.1)	2.2 (± 0.6)
FS-500	3268 (± 240)	25.9 (± 0.1)	2.3 (±0.2)
FF + FS-500	3303 (± 083)	28.7 (± 0.8)	3.4 (± 0.7)
FF	3668 (± 090)	33.0 (± 0.1)	5.5 (± 0.2)
WF	2907 (± 073)	27.7 (± 0.2)	4.7 (± 0.1)